UCRL- 98605
PREPRINT

Boltzmann Master Equation Analysis of Pre-Equilibrium Neutron Emission from Heavy-Ion Collisions at 35 MeV/Nucleon

B. A. Remington
M. Blann
A. Galonsky
L. Heilbronn
F. Deak
A. Kiss
Z. Seres

This paper was prepared for submittal to
Physical Review C

April 1988

Lawrence Livermore National Laboratory

Boltzmann Master Equation Analysis of Pre-Equilibrium Neutron Emission from Heavy-Ion Collisions at 35 MeV/nucleon

B.A. Remington and M. Blann
E-Division, L-280
Lawrence Livermore National Laboratory
Livermore, CA 94550

and

A. Galonsky and L. Heilbronn
National Superconducting Cyclotron Laboratory and
Department of Physics and Astronomy
Michigan State University, East Lansing, MI 48824-1321

and

F. Deak and A. Kiss
Department of Atomic Physics, Eotvos University
Puskin u. 5-7, Budapest, Hungary, H-1088

and

Z. Seres
Hungarian Academy of Sciences, Central Research Institute for Physics,
POB 49, Budapest 114, Hungary 1525

Abstract

The Boltzmann master equation model was used to study pre-equilibrium neutrons emitted in coincidence with light fragments from collisions of $^{14}N + ^{165}Ho$ at 35 MeV/nucleon. The input parameters of the model were adopted from earlier analyses of neutron spectra gated by evaporation residues at similar and somewhat lower incident energies. Both the shapes and the absolute magnitudes of the spectra of neutrons in coincidence with light fragments could be reproduced, provided a reduced excitation energy was used in the calculations. The energy removed from the excitation energy was equated with the collective energy of the intermediate state di-nuclear complex. For collisions leading to high energy fragments near the grazing angle, this collective energy corresponds to the kinetic energies above the Coulomb barrier of the projectile-like and target-like fragments in the center-of-mass system, assuming a binary reaction. For more strongly damped collisions, the spin rotational energies of the fragments was also included. This is qualitatively in agreement with a binary reaction where the energy held in collective modes of the intermediate state is unavailable for pre-equilibrium emission processes.

This work was performed under the auspices of the U. S. Department of Energy by the Lawrence Livermore National Laboratory under contract W-7405-Eng-48.

I. INTRODUCTION

The detection of pre-equilibrium (PE) nucleons is one of the most direct means of observing heavy-ion reaction dynamics early in the collision process. For incident energies as low as 13 MeV/nucleon, PE neutron multiplicities are near unity,[1] and at 30 MeV/nucleon, the value approaches 3.[2] A clear understanding of the PE emission process would offer a powerful tool for monitoring the early collision conditions for various reactions, such as fusion, fast fission, fragmentation, and transfer. Consequently, there has been keen interest in conducting experiments to measure PE emission under various controlled conditions[1-8] and in executing microscopic calculations to try to understand the fundamental mechanism behind the emission process.[8-15]

The PE emission process manifests itself in differential nucleon spectra as a forward-peaked, high energy component. Quite often a moving-sources prescription is used to decompose the spectra into various components, one of which is associated with PE emission and which typically is "hot".[1-5] The parameters of the "hot source" are then studied as a means of examining pre-equilibrium dynamics.[3-5]

In particular, we are intrigued by the source systematics reported in Refs. 4 and 5 for neutrons resulting from strongly damped and from peripheral collisions of ^{14}N at 35 MeV/nucleon on ^{165}Ho. We wish to re-examine these results within the framenwork of the Boltzmann master equation (BME) model for PE nucleon emission. For completeness, a description of the BME model is

presented in Section II. In Section III we discuss the preparation of the data to be compared with the BME calculations, namely, isolation of and angular integration of the PE component of the experimental spectra. The results of our calculations and comparisons with the experimental data are contained in Section IV. In Section V we present a discussion of a possible interpretation of our results, and our summary and conclusions are given in Section VI. A short discussion on the consequences of using a moving thermal source to parameterize PE nucleon spectra is given in the Appendix.

II. The Boltzmann Master Equation Model

The Boltzmann master equation model has been used with considerable success in reproducing both the shape and the absolute magnitude of PE neutron spectra from central collisions at incident energies of 10-30 MeV/nucleon.[14,15] In this study of strongly damped and peripheral collisions at 35 MeV/nucleon, we will adopt the input parameters to the BME model from such studies of central collisions. Our intention will be to relate deviations of the data from the calculation, if they occur, to the non-central nature of the reaction. In this section we describe the BME model as it has been formulated for central collisions.

The basic idea of a master equation stems from statistical physics[16] and asserts that the transition of particles into and out of given elements of phase space can be followed with a set of coupled differential equations. This approach was first applied to the nucleus by Harp, Miller and Berne[17] to

describe nucleon-induced PE reactions. The model was generalized by Blann to describe α-particle induced and heavy-ion induced nuclear collisions.[14,18] At the core of the BME model are a set of Boltzmann-like coupled differential equations describing the time rate of change of the number of nucleons/MeV at a given energy ϵ_i above the bottom of the nuclear well. (Henceforth, the energy ϵ_i will be denoted by its subscript, i.) These equations differentiate between neutrons and protons in a two-component Fermi gas and can be written as[14,17,18]

$$\frac{d^2N^x_{(\epsilon=\epsilon_i)}}{d\epsilon\, dt} = g_i^x \sum_y \sum_{jk\ell}{}' [\omega^{xy}_{k\ell\to ij}\, g_k^x g_\ell^y g_j^y n_k^x n_\ell^y (1-n_i^x)(1-n_j^y) - \omega^{xy}_{ij\to k\ell}\, g_j^y g_k^x g_\ell^y n_i^x n_j^y (1-n_k^x)(1-n_\ell^y)]\, \Delta\epsilon_j^y \Delta\epsilon_k^x \Delta\epsilon_\ell^y - g_i^x n_i^x \omega^x_{i\to i'} + f_i^x(t) \quad , \tag{1}$$

where the prime on the summation sign indicates the constraint due to energy conservation. The superscripts x and y indicate the species of nucleon, and the subscripts i,j,k, and ℓ denote the energy above the bottom of the nuclear well. g_i^x gives the density of single-particle levels at energy i for nucleons of type x, as calculated in the Fermi gas model. n_i^x denotes the time-dependent fraction of levels in a 1-MeV-wide bin at energy i which are occupied by a nucleon of type x, and the Pauli exclusion principle is embodied

in the $(1-n_i^x)$ factors. $\Delta\epsilon_j^y$ denotes the width of the energy bin of a y-type nucleon at energy j, and 1-MeV-wide bins have been used throughout. $\omega_{k\ell\rightarrow ij}^{xy}$ represents the transition rate for a nucleon of type x at energy k to scatter from a nucleon of type y at energy ℓ, yielding nucleons of energies i and j in the final state, where energy conservation requires that $i+j=k+\ell$. This transition rate can be written as[17,18]

$$\omega_{k\ell\rightarrow ij}^{xy} = \frac{\sigma_{k\ell}[2/m(\epsilon_k+\epsilon_\ell)]^{1/2}}{V \sum_{qr}' g_q^x g_r^y \Delta\epsilon_q^x \Delta\epsilon_r^y} \qquad (2)$$

where V is the nuclear volume, m is the nucleon mass, and $\sigma_{k\ell}$ is the free nucleon-nucleon scattering cross section for nucleons of energies k and ℓ above the bottom of the well. Perpendicular nucleon collision geometry is assumed and the cross sections are taken from the compilation of Arndt et al.[19] The summation in the denominator normalizes the transition rate to a specific (i,j) final state, as opposed to the rate for the two nucleons to scatter into any final state allowed by energy conservation. $\omega_{i\rightarrow i'}^x$, in Eq. 1 gives the rate of transmission of an x-type nucleon at energy i into the continuum at energy i'. These rates are calculated from the rate for the inverse reaction (capture of nucleon x at laboratory energy i' into the nucleus at energy i), making use of the reciprocity theorem and the method of Dostrovsky et al.[20] This continuum term is then integrated over time to predict the differential nucleon multiplicity spectrum:

$$\frac{dM^x_{(\epsilon=\epsilon_{i'})}}{d\epsilon} = \int (\Sigma_i \, g_i^x n_i^x \omega^x_{i\to i'}) dt \ . \qquad (3)$$

The last term in Eq. 1, $f_i^x(t)$, is the injection term, which gives the time dependent rate of insertion into the nuclear well of nucleons of type x at energy i from the projectile nucleus. The velocity of approach is assumed constant, and set equal to the nucleus-nucleus center-of-mass energy above the Coulomb barrier. The density of the fusing system is assumed to remain constant at the value corresponding to a square well with r_o=1.5 fm.

To start the nucleonic cascade process, as described by Eqs. 1 and 2, we need an initial distribution of nucleons, i.e., we need to define within the model the ground state of the two heavy nuclei. The target nucleus is assumed to be a Fermi gas at zero temperature. The projectile nucleus is, on the other hand, a Fermi gas in motion. We need to couple the intrinsic Fermi motion of the projectile nucleons to the relative motion of approach of the projectile nucleus. It has been pointed out that a simple coupling corresponding to shifted Fermi spheres in the infinite nuclear matter limit is not sufficient.[21] We have approached this problem drawing upon experience from treating precompound decay for nucleon and α-particle induced reactions.[18] We assume that the available entrance channel excitation energy is partitioned among only the projectile nucleons, with each energy-conserving configuration bearing equal a-priori weight. If we assume a constant single particle level density, g, then for a given energy E to be partitioned by n_o

nucleons, the number of possible configurations is given by an expression due to Ericson:[22]

$$N(n_o,E) = \frac{(gE)^{n_o-1}}{p!h!(n_o-1)!} \quad . \tag{4}$$

Here p and h are the initial number of particles and holes, jointly called excitons, and within our assumption, $n_o = p+h = A_{proj}$ and h=0. Assuming that each configuration bears equal a-priori weight, we obtain for the initial differential nucleon energy distribution

$$\frac{dn(\epsilon)}{d\epsilon}\Delta\epsilon = \int_{\epsilon'=\epsilon-\Delta\epsilon/2}^{\epsilon+\Delta\epsilon/2} \frac{N(n_o-1,E-\epsilon')}{N(n_o,E)}\, g\, d\epsilon'$$

$$= \frac{n_o[(E-\epsilon+\Delta\epsilon/2)^{n_o-1} - (E-\epsilon-\Delta\epsilon/2)^{n_o-1}]}{E^{n_o-1}} \quad , \tag{5}$$

where $\Delta\epsilon$ is the width of the energy bins in the calculation. In our use of Eqs. 4 and 5, we assume that the energy partitioned is the excitation energy that would be available if a compound nucleus were formed, i.e., the center-of-mass energy plus the Q value for fusion.

In summary, the initial projectile nucleon energy distribution assumed is given by Eq. 5. These nucleons are injected in a time dependent fashion into the target nuclear well. The relaxation process due to nucleon-nucleon collisions is described by Eqs. 1 and 2, and the final nucleon emission spectrum results from Eq. 3.

III. Preparation of the Data

The experimental data to be studied in this work stem from an experiment measuring neutrons in coincidence with light fragments near and beyond the grazing angle for $^{14}N + ^{165}Ho$ collisions at 35 MeV/nucleon. This experiment has been reported in Ref. 4, and the complete data set can be found in Ref. 23. Comprehensive analyses of an earlier though very similar experiment are reported in Refs. 24-27. Samples of the data from Ref. 23 are shown in Figs. 1 and 2. For ease of notation, we will refer to the detected coincident light fragment as the projectile-like fragment (PLF), without regard to whether or not the fragment retains memory of the entrance channel. For each coincident PLF angle and species, two energy gates were set: one for low energy and one for high energy PLFs. The energy gates used are listed in Table 1, together with the inclusive PLF cross sections and the average PLF energy for each gate. As a visual aid, an inset is included in each figure showing the PLF energy spectrum and indicating the gate with hatching. More detailed information on the PLF spectra can be found in Refs. 4, 5 and 27.

Figure 1 shows the neutron differential multiplicity spectra in the lab frame at 10 angles associated with a low energy lithium PLF detected at +23°. The lithium energy spectrum and the gated region are shown in the inset. The open circles are for neutrons detected on the same side of the beam as the coincident PLF, and "same-side" neutron angles are designated as positive ("opposite-side" neutron angles being negative). The steeply falling, nearly isotropic low energy component of the spectra corresponds to neutrons

evaporated from a slowly moving heavy target-like fragment (TLF).[3-5,28] The "hard" (nearly flat), high energy component of the neutron spectra corresponds to PE emission. The curves result from a moving thermal sources analysis of the data[4,23] and will be discussed separately in the Appendix. The enhancement in the "same-side" +30° neutron spectrum (open circles) centered at 10 MeV [as compared with the "opposite-side" -30° spectrum (closed squares)] corresponds to low energy neutrons emitted from discrete states of the lithium PLF moving on the average at about 10 MeV/nucleon towards the +23° fragment telescope. Kinematic focusing results in the observed enhancement.[24-26]

Figure 2 presents neutron multiplicity spectra in coincidence with high energy lithium PLFs at +10°. The same components discussed in Fig. 1 are also present here. The contribution due to PLF sequential decay is larger due to the greater kinematic focusing from the colinear geometry of the neutron and fragment detectors, both at +10°.

For reasons discussed in the Appendix, the moving sources parameterization will not be used to extract the PE component of the neutron spectra. Instead, we will deal with the data directly in a five-step preparation process. The first two steps are as follows: (1) To isolate the PE neutron component from the low temperature evaporative TLF component, we limit our study to neutrons with energies of or exceeding 20 MeV. The contamination of the high energy neutron multiplicity from low temperature TLF neutrons is negligible. (2) To remove the component from PLF sequential decay, we make use of the fact that neutron detectors were placed at symmetric angle

pairs. At energies and angles where noticeable PLF sequential decay was observed (as evidenced by an enhancement of the "same-side" neutron spectrum over the corresponding "opposite-side" spectrum), we used the "opposite-side" spectrum to represent the true PE component. For the ±10° neutron spectra, there were some cases where even the "opposite-side" spectrum had a small contamination from PLF sequential decay. This was observed as a shoulder in an otherwise smoothly varying angular distribution, and was not included in the PE component of the neutron spectrum.

Since the BME model is constructed in energy space, it predicts nucleon energy spectra, but has no angular information. Therefore, as the third and fourth steps in the data preparation, the experimental differential multiplicity spectra need to be integrated over polar and azimuthal angles. Figures 3 and 4 show the PE neutron (polar) angular distributions in the lab frame for the spectra shown in Figs. 1 and 2, respectively. The neutron energies selected are 20, 40, 60, 80 and 100 MeV, and the coincident lithium energy spectra and gated regions are shown in the insets. The error bars represent the estimated uncertainty in the data rebinning process, and the curves serve as an aid in the extrapolation to large and small angles. The angular distributions are in general smooth and nearly exponential in shape, and tend to increase in steepness with increasing neutron energy. The angular distributions of neutrons in coincidence with high energy lithium PLFs (Fig. 4) are slightly steeper than those for low energy lithiums (Fig. 3).

In integrating these data over polar angle (step 3), the data points were joined using an exponential function, and the extrapolation to 0° and 180° was accomplished by visually fitting smooth curves through the locus of points.

The solid lines in Figs. 3 and 4 are for neutron spectra gated by Li fragments, but those gated by Be, B, and C have very similar extrapolation curves.

The fourth step, integration over azimuthal angle, is complicated by the azimuthal asymmetries which PE nucleon emission spectra for this and similar systems have been shown to exhibit. If the reaction plane is defined by the beam axis and the direction of the scattered PLF, then more high energy nucleons have been observed in this plane, as opposed to the plane perpendicular to it.[5,28-30] Therefore, in carrying out the integrations over solid angle, this azimuthal asymmetry needs to be taken into account. To do this we use the empirical azimuthal parameterization of Bloch et al.,[29] in conjunction with the measured in-plane to out-of-plane PE neutron multiplicity ratios of Refs. 5 and 28. We find that the angle-integrated neutron spectra corresponding to a coincident PLF at 10° and at 23° need to be reduced by 10% and by 25%, respectively, from results where this azimuthal asymmetry is neglected.

The angle-integrated differential neutron multiplicities were generated for a low energy (LE) and a high energy (HE) gate on PLF elements of Li, Be, B, and C at 23° and at 10°. These are displayed in the lab frame in Figs. 5-8 as various open symbols for the different PLF species. The manner in which the angular distributions were extrapolated to back angles becomes important for high neutron energies. The uncertainty inherent in this process was estimated and given as an error bar for the 100 MeV data points, which represent the worst cases. At the lower energies, in cases where significant

filtering of PLF sequential decay neutrons was necessary, the uncertainty introduced was also estimated and given as error bars. In examining Figs. 5-8, the angle-integrated PE neutron spectra seemed largely independent of the species of coincident PLF. Therefore, only the experimental results averaged over PLF species, shown by the solid plotting symbols, are compared with the BME calculations. The PLF singles cross sections for each species and gate, as given in Table 1, were used as weighting factors in the averaging.

Since the BME calculations take place in the nucleus-nucleus center-of-mass (CM) frame, the fifth and final step of the data preparation is to transform the data into the CM frame. The solid symbols in Figs. 5-8, which have been averaged over PLF species, have also been transformed into the CM frame.

IV. Comparisons of Calculated and Experimental Results

For the collisions under investigation in the following, the prescription for setting the input parameters of the BME, as described in Section II, have to be reconsidered. Specifically, for centrally gated data the excitation energy used is that of the compound nucleus, and the entire projectile nucleus is assumed to participate, i.e., $n_o = A_{proj}$. For data gated by PLFs from peripheral collisions, however, these assumptions may not be valid. To constrain the amount of parameter adjustment in this first analysis of peripheral collisions with the BME model, the only input parameter that will be varied is the degree of damping, i.e., the excitation energy assumed in the

calculation. The results of calculations for five values of excitation energy are shown as solid curves, each for n_o = 14 initial excitons. In each figure the top curve, labeled 1, is for the full center-of-mass excitation energy plus Q value for fusion, namely E^*_o = 440 MeV. Curves 2-5 correspond to calculations with the excitation energy decreased by 50, 100, 150, and 200 MeV, respectively.

Figure 5 shows the experimental neutron spectra in coincidence with low energy fragments at 23°. The inset shows a typical fragment spectrum and energy gate (boron), and Table 1 lists the gates used for each fragment species. Examination of the fragment spectrum in the inset shows that the fragments in the gate are emerging at or somewhat above the Coulomb barrier. Comparing the calculations only with the experimental results averaged over PLF species, the data appear to fall between curves 2 and 3. The gate on fragment energies not far from the Coulomb barrier and at angles well beyond the grazing angle presumably selects "hard", nearly fully damped collisions. But the resulting neutron spectrum has a slope somewhat "softer" (steeper) than would be expected for a central collision leading to an evaporation residue (curve 1). One interpretation of this effect is that a sizeable amount of the center-of-mass energy is not available for the processes responsible for PE neutron emission.

A recent result by Bloch et al.[29] reported on measurements of neutrons in coincidence with light fragments at larger angles (50°-90°). In comparisons of the neutron energy spectra with predictions of the BME model, it was found that their data also had a slightly "softer" slope than the

standard ($n_o = A_{proj}$) calculation. The authors pointed out, though, that either a reduction in the total excitation energy assumed in the calculation or an increase in the initial exciton number, n_o, would achieve similar results and bring the calculations into agreement with the data. Since BME analyses of centrally gated collisions have been quite successful using $n_o = A_{proj}$,[14,15] we choose in this analysis not to vary n_o.

In Fig. 6 we show the neutron spectra in coincidence with high energy fragments at 23°. The solid curves corresponding to the BME calculations are the same as in Fig. 5. There appears to be a distinct steepening of the slope of the experimental spectrum. The higher energy neutrons fall between curves 4 and 5, indicating that as the energy of the PLF increases, the PE neutron spectrum becomes "softer".

Figure 7 shows the neutron spectra in coincidence with low energy fragments at 10°. It is interesting to notice that the experimental spectra of Figs. 6 and 7 are very similar, with the yield of higher energy neutrons falling between curves 4 and 5. The average energies of the coincident light fragments, though, are quite different: from Table 1 we see that for Fig. 7 the average fragment energy is 95 MeV whereas for Fig. 6 the value is 171 MeV. We expect that this reflects a mix of reaction mechanisms selected by the PLF energy gates of Figs. 6 and 7. As such, these two figures represent transitional regions. Instead of further examination of these transitional results, we turn to the cleaner reaction trigger of high energy PLFs near the grazing angle.

Figure 8 shows the neutron spectra in coincidence with high energy fragments at 10°, as compared to the grazing angle of about 8°. The gated region of the fragment spectrum is reasonably broad, including both the near beam velocity component, typically referred to as quasi-elastic,[27] and fragments moving somewhat slower than beam velocity. Similar to Figs. 6 and 7, these neutron spectra appear to have a steep slope, with the highest energy neutrons falling near curve 5. Based on the interpretation adopted in the discussion of Fig. 5, it would appear that a large amount of energy is not available for PE nucleon emission. Presumably this energy is held in collective degrees of freedom and eventually emerges as the energy of the detected coincident PLF.

V. Discussion and Interpretation

To develop a detailed, microscopic interpretation of the PE neutrons produced in coincidence with PLFs would require both an understanding of the fragment emission process as well as PE nucleon emission. Such a level of fundamental understanding is beyond the scope of currently available models. Instead, we opt for a more qualitative and phenomenological approach. We will limit our considerations in the following to the two extreme cases, shown by Figs. 5 and 8.

We start by considering the results of Fig. 8 for PE neutrons in coincidence with high energy fragments near the grazing angle. The essence of the BME picture of PE nucleon emission is that some fraction of the entrance

channel collective (projectile) energy is converted into random excitation energy. Conversely, emission of fragments at high energies into the forward angles is a very ordered, collective process. It would appear to us that energy and nucleons once randomized (hence, becoming available for PE nucleon emission processes) would not with any large probability re-coalesce some time later as the observed high energy PLF at near grazing angles. Therefore, we propose that the energy which is observed as the kinetic energy of the PLF was, during the actual nuclear collision time, unavailable for PE nucleon emission processes. This should also be true for the unobserved TLF. We define this unavailable energy as collective energy, and write

$$E_{collective} = E^{c}_{PLF} + E^{c}_{TLF} - V_{C} \quad , \tag{9}$$

where E^{c}_{PLF} and E^{c}_{TLF} are the average PLF and TLF kinetic energies in the CM system, and V_{C} is the Coulomb barrier. The averages are taken first over the extent of the PLF energy gate for each PLF species, and then over the four species of PLF. In averaging over the energy gate, the weighting function used was the PLF singles cross section. In princple the PLF coincidence cross section should be used as the weighting function, but this information was not available. This caveat will be kept in mind when interpreting our results. To estimate the TLF kinetic energies, we adopt a binary hypothesis, namely, Projectile + Target → PLF + TLF, and rely on conservation of momentum. For PE neutrons in coincidence with high energy PLFs near the grazing angle, the

values of $E_{collective}$ are listed at the top of Table 2. We thus estimate that for the neutron spectrum of Fig. 8, $E_{collective}$ = 216 MeV, and this energy was unavailable for PE nucleon emission. The calculation corresponding to curve 5 in Fig. 8, which is in reasonable agreement with the data, corresponds to an excitation energy of E_o^* - 200 MeV, i.e., 200 MeV was assumed unavailable for PE nucleon emission. Bearing in mind the caveat concerning use of the PLF singles cross sections as the weighting function, this level of agreement seems quite promising. Our conclusion for PE neutron emitted in coincidence with high energy fragments at forward angles is that the BME model gives a good prediction of <u>both</u> the absolute magnitude <u>and</u> the shape of the spectrum, provided that the collective energy is removed from the PE nucleon emission process.

We next turn to the results of Fig. 5 for PE neutron emission in coincidence with low energy fragments at 23°. Once again we will assume that the collective energy which eventually emerges as the kinetic energy of the PLF and TLF was unavailable for PE nucleon emission processes. In other words, we assume that a PLF coalescence scenario is <u>still</u> not applicable to these data. This assumption is experimentally backed by a detailed coalescence model analysis of the singles fragments resulting from this system at 30°.[27] In that analysis, the coalescence model was unsuccessful for fragments heavier that α particles. The values for the collective energies corresponding to Fig. 5 are listed at the bottom of Table 2, and we find that $E_{collective}$ = 13 MeV. Using E_o^* - 13 MeV in a BME calculation would give a

result just slightly below curve 1. Though such a prediction would fall within the error bars of the data, it would still lie slightly above the centroid of the distributions giving rise to the solid points. Therefore, we consider the possiblilty that some additional mechanism is converting entrance channel energy into collective energy. Notably, we have not yet considered whether energy is transformed into the spin rotational energy of the PLF and TLF. For the "harder" collisions giving rise to low energy PLFs at 23°, perhaps there is sufficient tangental friction[32,33] to convert non-negligible amounts of entrance channel energy into spin rotational energies.

To make a rough estimate of where such a scenario might lead, we turn to the semi-classical scattering model of Bass.[34] We appy this model to the system under study, and the resulting partial wave decomposition of the reaction cross section is shown in Fig. 9. Assuming that Fig. 5 represents an inelastic reaction, then from Fig. 9 we see that $79 < \ell < 134$, where ℓ is the entrance channel orbital angular momentum quantum number. Guessing a representative value of $\ell \approx 110$ and adopting the "rolling" limit[33] for the collision (which is consistent with the assumptions of the semi-classical model of Bass[34]), we can estimate the amount of entrance channel angular momentum, ℓ_o, converted into spin angular momenta of the PLF and TLF. From Ref. 33, we have in the "rolling" limit that $I_{PLF} + I_{TLF} = (2/7)\ell_o$, where $I_i = R_i/(R_{PLF} + R_{TLF})$, and i represents either the PLF or TLF. Then using rigid spherical rotors (and $r_o = 1.2$ fm), we estimate the sum of the spin rotational energies of the PLF and TLF, averaged over PLF, TLF species, to be 81 MeV.

Implicit in the calculation is our assumption that the binary reaction, Projectile + Target → PLF + TLF, occurred prior to the onset of the tangental frictional force. If we reverse this time sequence and assume that tangental friction causes the projectile to "roll", followed by the binary reaction, then the sum of the spin energies is 44 MeV. Since we do not know which occurs first, we take the average, namely, 62 MeV. Therefore,

$$E_{collective} = E^{c}_{PLF} + E^{c}_{TLF} - V_{C} + E^{Rot}_{PLF} + E^{Rot}_{TLF} \quad , \qquad (10)$$

which gives $E_{collective}$ = 13 + 62 = 75 MeV. If 75 MeV were removed from the excitation in the calculations of Fig. 5, this would produce a prediction between curves 2 and 3, in good agreement with the data.

We return once again to the results of Bloch et al.[29] for PE neutrons in coincidence with PLFs at 50°-90°. In that work, the excitation energy assumed in a BME analysis needed only to be reduced by the kinetic energy of the PLFs. In other words, no spin rotational energy was assumed. We speculate that in collisions leading to fragments at such large angles, perhaps the "sticking" limit has been reached.[33] In this limit the spin angular momenta, and hence, spin rotational energies of the PLF and TLF are much smaller than for the "rolling" limit, and might indeed be negligible compared to the kinetic energies.

VI. Summary and Conclusion

We have studied PE neutron emission for ^{14}N + ^{165}Ho collisions at 35 MeV/nucleon gated by light fragments of various energies and at angles ranging from 7° to 30°. For fragments at a given angle and in a given kinetic energy gate, the experimental neutron spectra were essentially independent of the species of the coincident fragment. At a given angle, the lower the energy of the coincident fragment, the flatter the slope of the PE neutron energy spectra.

We have analyzed the data within the framework of the Boltzmann master equation model. All of the experimental results can be reproduced quite well by adjusting only the available excitation energy. Neutron spectra corresponding to coincident high energy fragments near the grazing angle can be reproduced both in shape and absolute magnitude within the BME model provided collective energy is "removed" from the calculation. Assuming a binary reaction, this collective energy is equated with the center-of-mass kinetic energies of the PLF and TLF above the Coulomb barrier. For low energy fragments at 23° and 30°, we also included the spin rotational energies of the fragments as collective energy to obtain good agreement with the data.

These observations are in qualitative agreement with a binary reaction scenario where the energy which eventually emerges as kinetic energy above the Coulomb barrier of the PLF and TLF was unavailable for PE emission during the actual collision process. This energy presumably was held in the collective motion of the di-nuclear complex of the intermediate state. For very

peripheral collisions leading to high energy fragments near the grazing angle, only the PLF and TLF kinetic energies needed to be considered, consistent with a "slipping" collision. For low PLF energies at angles somewhat larger than the grazing angle, a "rolling" collision was assumed, with the implication that additional collective energy was held as the spin rotational energies of the PLF and TLF. For collisions leading to low energy fragments at large angles, a "sticking" assumption might apply, with the spin rotational energies being small compared to their kinetic energies. A more quantitative test of this idea will have to await future work. Perhaps then a unified picture of PE emission dynamics can be established, spanning central, strongly damped and peripheral collisions.

VI. Appendix: PE Emission and the "Hot Source"

The trend mentioned in Section III concerning Figs. 3 and 4, namely, that the higher the energy of the coincident PLF, the steeper the slope of the PE neutron energy spectrum, was missed in a previous, moving thermal sources analyses of these data.[4,23] The observation that the angular distributions of PE neutrons from peripheral collisions (Fig. 4) are slightly steeper than those from strongly damped collisions (Fig. 3) was overlooked as well. Furthermore, close scrutiny of Figs. 1 and 2 shows that the moving sources fits are underpredicting the high energy neutron multiplicities at 10° and 30°. These oversights reflect the fact that there are limits to which a single moving source can reproduce PE nucleon energy spectra.

The PE component of a nucleon spectrum results from nucleons emitted after 0, 1, 2, 3, ... nucleon-nucleon collisions, until equilibrium is established. If thermal sources are invoked to parameterize PE emission, each collisional "order" would correspond to a source of given mass, temperature, and velocity.[35] A summation over the emission from all of these sources would then yield the final PE spectrum. The convenience of using a single thermal source to parameterize the entire PE component is certainly appealing. The consequence for such convenience, though, is that details of PE emission dynamics and systematics will be overlooked, and only coarse trends will be observed.[36] For categorizing large bodies of data, coarse trends may be sufficient. But for a detailed study of PE emission dynamics, this is not acceptable.

The support of the U.S. National Science Foundation under Grants PHY-86-11210 and INT-86-17683 and of the Hungarian Academy of Sciences is gratefully acknowledged. It is a pleasure to thank R. Vandenbosch, W.U. Schroder, D.J. Fields, and C. Bloch for helpful discussions. We also thank J. Cramer for making his heavy-ion optical model available to us. One of us (B.A.R.) wishes to acknowledge the warm hospitality received at the National Superconducting Cyclotron Laboratory at Michigan State University, where part of this work was conducted.

References

1) A. Gavron, A. Gayer, J. Boissevain, H.C. Britt, T.C. Awes, J.R. Beene, B. Cheynis, D. Drain, R.L. Ferguson, F.E. Obenshain, F. Plasil, G.R. Young, G.A. Petitt, and C. Butler, Phys. Rev. C 35, 579 (1987)

2) D. Hilscher, H. Rossner, A. Gamp, U. Jahnke, B. Cheynis, B. Chambon, D. Drain, C. Pastor, A. Giorni, C. Morand, A. Dauchy, P. Stassi, and G. Petitt, Phys. Rev. C 36, 208 (1987).

3) G. Caskey, A. Galonsky, B. Remington, M.B. Tsang, C.K. Gelbke, A. Kiss, F. Deak, Z. Seres, J.J. Kolata, J. Hinnefeld, and J. Kasagi, Phys. Rev. C 31, 1597 (1985).

4) B.A. Remington, G. Caskey, A. Galonsky, C.K. Gelbke, L. Heilbronn, F. Deak, A. Kiss, Z. Seres, J. Kasagi, and J.J. Kolata, Phys. Rev. C 34, 1685 (1986).

5) F. Deak, A. Kiss, Z. Seres, G. Caskey, A. Galonsky, C.K. Gelbke, B. Remington, M.B. Tsang, and J.J. Kolata, Nucl. Phys. A464, 133 (1987).

6) C. Bloch, W. Benenson, A.I. Galonsky, E. Kashy, J. Heltsley, L. Heilbronn, M. Lowe, B. Remington, D. Morrissey, and J. Kasagi, Phys. Rev. C 36, 203 (1987).

7) H.J. Rabe, K.D. Hildenbrand, U. Lynen, W.F.J. Muller, H. Sann, H. Stelzer, W. Trautmann, R. Trockel, R. Wada, J. Pochodzalla, E. Eckert, P. Kreutz, A. Kuhmichel, N. Brummund, R. Glasow, K.H. Kampert, R. Santo, D. Pelte, G.S.I. Preprint No. GSI-87-19, 1987.

8) W. Rosch, W. Cassing, H. Gemmeke, R. Gentner, K. Keller, L. Lassen, W. Lucking, A. Richter, R. Schreck, and G. Schrieder, Phys. Lett. 197B, 19 (1987).

9) William A. Friedman, Phys. Rev. C 29, 139 (1984).

10) J. Randrup and R. Vandenbosch, Lawrence Berkeley Laboratory Preprint No. LBL-23359, 1987.

11) A. Iwamoto, Phys. Rev. C 35, 984 (1987).

12) K.R.S. Devi, M.R. Strayer, K.T.R. Davies, S.E. Koonin and A.K. Dhar, Phys. Rev. 24, 2521 (1981).

13) W. Bauer, G.D. Westfall, D. Fox, D.A. Cebra, M.S.U. Cyclotron Preprint No. MSUCL-570, 1986.

14) M. Blann, Phys. Rev. C 31, 1245 (1985); M. Blann, in Proceedings of the Symposium on the Many Facets of Heavy- Ion Fusion Reactions, March 1986, p. 285, Argonne National Laboratory Report ANL-PHY-86-1; M. Blann, Phys. Rev. C 35, 1581 (1987).

15) M. Blann and B.A. Remington, in Proceedings of the Texas A&M Symposium on Hot Nuclei, World Scientific, in press; ibid., Lawrence Livermore National Laboratory Report No. UCRL-97722, 1987.

16) F. Reif, Fundamentals of Statistical and Thermal Physics, (MaGraw-Hill, San Francisco, 1965), pg. 548.

17) G.D. Harp, J.M. Miller and B.J. Berne, Phys. Rev. 165, 1166 (1968); G.D. Harp and J.M. Miller, Phys. Rev. C 3, 1847 (1971).

18) M. Blann, Ann. Rev. Nucl. Sci 25, 123 (1975); M. Blann, A. Mignerey and W. Scobel, Nukleonika 21, 335 (1976); M. Blann, Phys. Rev. C 23, 205 (1981).

19) R.A. Arndt, Phys. Rev. D 35, 128 (1987); R.A. Arndt et al., Phys. Rev. D 28, 97 (1983); B.J. VerWest and R.A. Arndt, Phys. Rev. C 25, 1979 (1982); M.L. Barlett et al., Phys. Rev. C 27, 682 (1983); R.A. Arndt, private communication, 1987.

20) I. Dostrovsky, Z. Fraenkel, and G. Friedlander, Phys. Rev. 116, 683 (1960).

21) W. Cassing, Z. Phy. A 326, 21 (1987); Z. Phys. A 327, 87 (1987).

22) T.E.O. Ericson, Adv. Phys. 9, 423 (1959).

23) B.A. Remington, Doctoral Thesis, Michigan State University Physics Department, 1986.

24) A. Galonsky, G. Caskey, L. Heilbronn, B. Remington, H. Schelin, F. Deak, A. Kiss, Z. Seres, J. Kasagi, Phys. Lett. B197, 511 (1987).

25) F. Deak, A. Kiss, Z. Seres, G. Caskey, A. Galonsky, and B. Remington, Nucl. Instrum. Meth. A258, 67 (1987).

26) A. Kiss, F. Deak, Z. Seres, G. Caskey, a. Galonsky, L. Heilbronn, B. Remington, and J. Kasagi, Phys. Lett. B 184, 149 (1987).

27) G. Caskey, L. Heilbronn, B. Remington, A. Galonsky, F. Deak, A. Kiss, and Z. Seres, Phys. Rev. C 37, 969 (1988)

28) A. Kiss, F. Deak, Z. Seres, G. Caskey, A. Galonsky, L. Heilbronn, and B. Remington, submitted to Phys. Rev. C for publication; M.S.U. Cyclotron Report No. MSUCL-636 (1988).

29) C. Bloch, W. Benenson, A.I. Galonsky, E. Kashy, J. Heltsley, L. Heilbronn, M. Lowe, R.J. Radtke, B. Remington, J. Kasagi, and D.J. Morrissey, M.S.U. Cyclotron Preprint, submitted to Phys. Rev. C for publication (1988).

30) D.J. Fields, W.G. Lynch, T.K. Nayak, M.B. Tsang, C.B. Chitwood, C.K. Gelbke, R. Morse, J. Wilczynski, T.C. Awes, R.L. Ferguson, F. Plasil, F.E. Obenshain, and G.R. Young, Phys. Rev. C 34, 536 (1986).

31) D. Hilscher, J.R. Birkelund, A.D. Hoover, W.U. Schroder, W.W. Wilke, J.R. Huizenga, A.C. Mignerey, K.L. Wolf, H.F. Breuer, and V.E. Viola, Jr., Phys. Rev. C 20, 576 (1979).

32) R. Beck and D.H.E. Gross, Phys. Lett. 47B, 143 (1973).

33) W.U. Schroder and John R. Huizenga, in Treatise on Heavy-Ion Science, Vol. 2, edited by D. Allen Bromley (Plenum Press, New York, 1984), p. 140.

34) R. Bass, Phys. Lett. 47B, 139 (1973); R. Bass, Nucl. Phys. A231, 45 (1974).

35) M. Blann and B. Remington, to appear in Phys. Rev. C 37 (1988); L.L.N.L. Preprint No. UCRL-97306 (1987).

36) C. Bloch and E. Kashy, Phys. Rev. C 36, 855 (1987).

Figure Captions

Figure 1. Neutron differential multiplicity spectra at 10 angles in coincidence with low energy lithum PLFs at +23° for collisions of $^{14}N + ^{165}Ho$ at 35 MeV/nucleon. The open symbols represent the positive neutron angles, and correspond to the same side of the beam axis as the detected PLF. Spectra below the top pair have been offset by successive factors of 100. The inclusive PLF energy spectrum and gated region are given in the inset. The curves are the result of a two moving sources parameterization. The slow moving (target like fragment) (TLF) had fit parameters of M_{TLF}= 7.5 neutrons, E/A_{TLF}= 0.07 MeV, T_{TLF}= 2.7 MeV, and θ_{TLF}= -14.4° for the total multiplicity, kinetic energy/nucleon, temperature, and angle, respectively. The faster moving "hot source" (HS) had parameters of M_{HS}= 2.3 neutrons, E/A_{HS}= 5.2 MeV, T_{HS}= 10.5 MeV, and θ_{HS}= 2.3°.

Figure 2. Same as Fig. 1 except that the coincident PLFs have low energy and are at +10°. The corresponding fit parameters from the moving sources parameterization were M_{TLF}= 5.3 neutrons, E/A_{TLF}= 0.07 MeV, T_{TLF}= 2.6 MeV, θ_{TLF}= -11.6°; M_{HS}= 1.7 neutrons, E/A_{HS}= 4.8 MeV, T_{HS}= 9.0 MeV, and θ_{HS}= 4.0°.

Figure 3. Pre-equilibrium neutron lab angular distributions for five neutron energies corresponding to the data of Fig. 1. The inclusive lithium PLF energy spectrum and gated region is shown in the inset. The distributions

have been offset by factors of 10, with the distribution at the top having no offset. The alternating plotting symbols are introduced only for clarity of presentation. The curves represent "visual fits" to the data and were used (in an integration over angle) to extrapolate to 0° and to 180°.

Figure 4. Same as Fig. 3 except that the corresponding data are those of Fig. 2.

Figure 5. Angle integrated neutron spectra in coincidence with low energy fragments of Li, Be, B, and C at 23°. The inset gives one of the inclusive fragment energy spectra (boron) and illustrates the gate. The open plotting symbols correspond to lab energy spectra and differentiate between the different fragment species, as given in the legend. The solid symbols, offset by a factor of 100, are the neutron spectra transformed into the center of mass system and averaged over fragment species. The error bars on the open symbols reflect the estimated errors resulting from integrating a limited angular distribution over angle and from contamination by PLF sequential decay neutrons. The error bars on the solid symbols represent the standard deviation of the group of four open symbols used in the average. Curves 1-5 correspond to the BME calculations with 0, 50, 100, 150 and 200 MeV removed from the compound nucleus excitation energy. All calculations assume $n_o = A_{proj} = 14$.

Figure 6. Same as Fig. 5 except that the neutrons are in coincidence with high energy fragments at 23°.

Figure 7. Same as Fig. 5 except that the neutrons are in coincidence with low energy fragments at 10°.

Figure 8. Same as Fig. 5 except that the neutrons are in coincidence with high energy fragments at 10°.

Figure 9. The partial wave decomposition of the reaction cross section within the semi-classical model of R. Bass.[34] In this model, for partial waves larger than about ℓ=134, the collision corresponds to quasi-elastic reactions. The upper limit of ℓ=161 was established as the grazing partial wave in a calculation with the heavy-ion optical model of J. Cramer. For the small partial waves, $\ell < 79$, the reaction proceeds via fusion and fusion-like processes. The intermediate partial waves, $79 < \ell < 134$ correspond to the regime of inelastic scattering. The representative value used in the inelastic collision analysis in the text, $\ell = 110$, is also marked.

Table 1. Energy gates set on the coincident fragments. ΔE_L corresponds to the low energy gate and ΔE_H to the high energy gate. The fragment cross sections and average energies are taken from the fragment singles data.

θ_{PLF}= 23°

PLF	ΔE_L(MeV)	$\frac{d\sigma}{d\Omega}$(mb/sr)	<E>(MeV)	ΔE_H(MeV)	$\frac{d\sigma}{d\Omega}$(mb/sr)	<E>(MeV)
Li	30- 96	75	64	100-260	65	147
Be	30-114	28	71	120-340	22	181
B	34-140	27	82	180-380	12	244
C	40-140	18	79	200-400	5	266
Average			70			171

θ_{PLF}= 10°

PLF	ΔE_L(MeV)	$\frac{d\sigma}{d\Omega}$(mb/sr)	<E>(MeV)	ΔE_H(MeV)	$\frac{d\sigma}{d\Omega}$(mb/sr)	<E>(MeV)
Li	31-105	120	74	136-220	426	181
Be	52-126	42	90	168-315	241	240
B	73-168	40	124	210-399	436	315
C	94-210	28	153	252-472	630	385
Average			95			297

Table 2. Average values for the center-of-mass energies of the PLF and TLF, where the TLF energies are calculated within the binary reaction assumption. The Coulomb barrier, V_c, is calculated using $r_o = 1.2$ fm, and the energy assumed to be held in collective motion of the di-nuclear complex is given by $E_{collective} = E^c_{PLF} + E^c_{TLF} - V_C$.

$\theta_{PLF} = 10°$, high energy gate:

PLF	E^c_{PLF}(MeV)	E^c_{TLF}(MeV)	V_C(MeV)	$E_{collective}$(MeV)
Li	151	6	33	124
Be	200	10	43	167
B	264	17	52	229
C	326	23	62	287
Average	250	15	50	216

$\theta_{PLF} = 23°$, low energy gate:

PLF	E^c_{PLF}(MeV)	E^c_{TLF}(MeV)	V_C(MeV)	$E_{collective}$(MeV)
Li	48	2	33	17
Be	52	3	43	11
B	59	4	52	11
C	55	4	62	0
Average	52	3	42	13

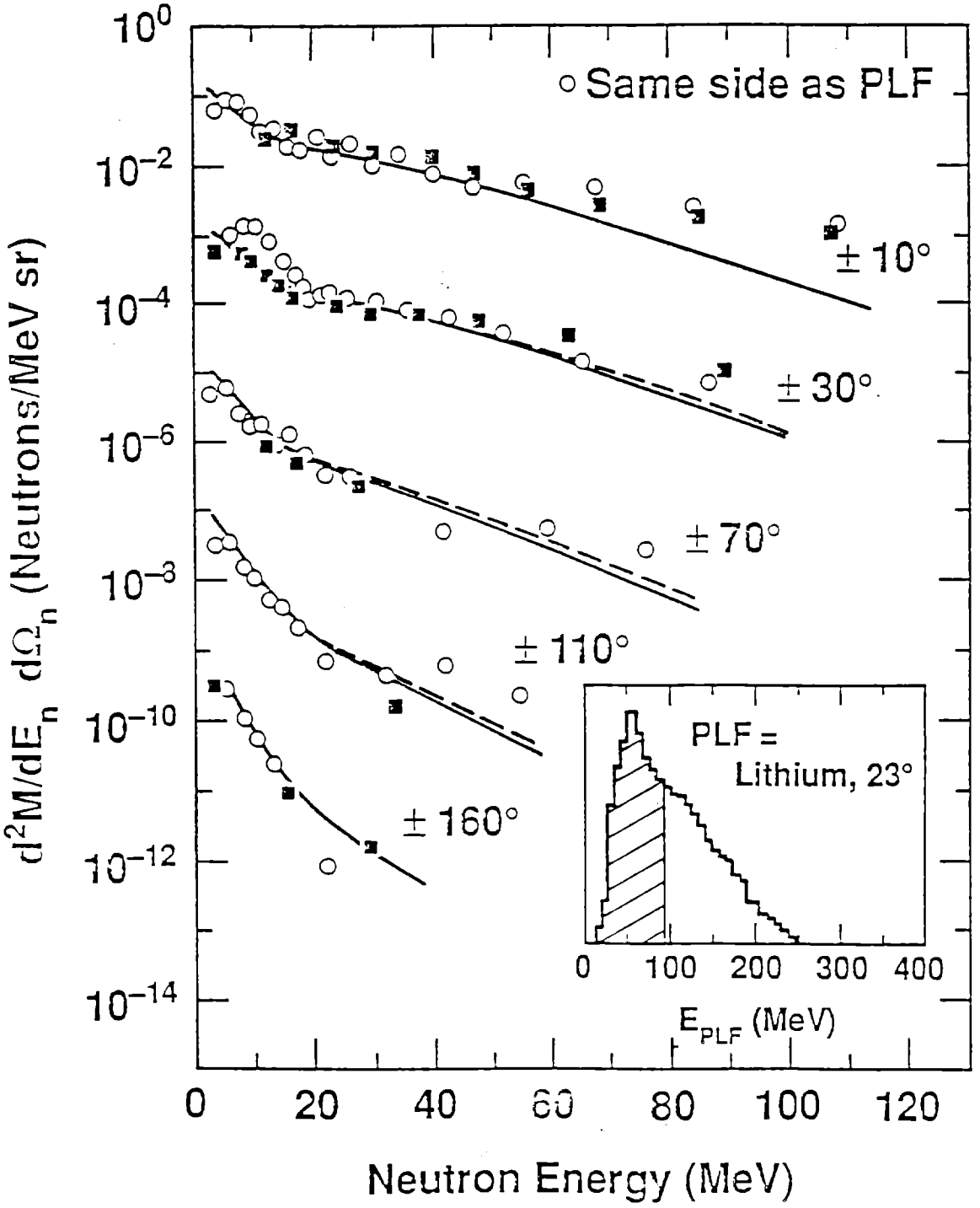
Same side as PLF
± 10°
± 30°
± 70°
± 110°
± 160°
PLF = Lithium, 23°
0 100 200 300 400
E_{PLF} (MeV)
$d^2M/dE_n\ d\Omega_n$ (Neutrons/MeV sr)
Neutron Energy (MeV)
0 20 40 60 80 100 120
10^0 10^{-2} 10^{-4} 10^{-6} 10^{-8} 10^{-10} 10^{-12} 10^{-14}

Fig 1

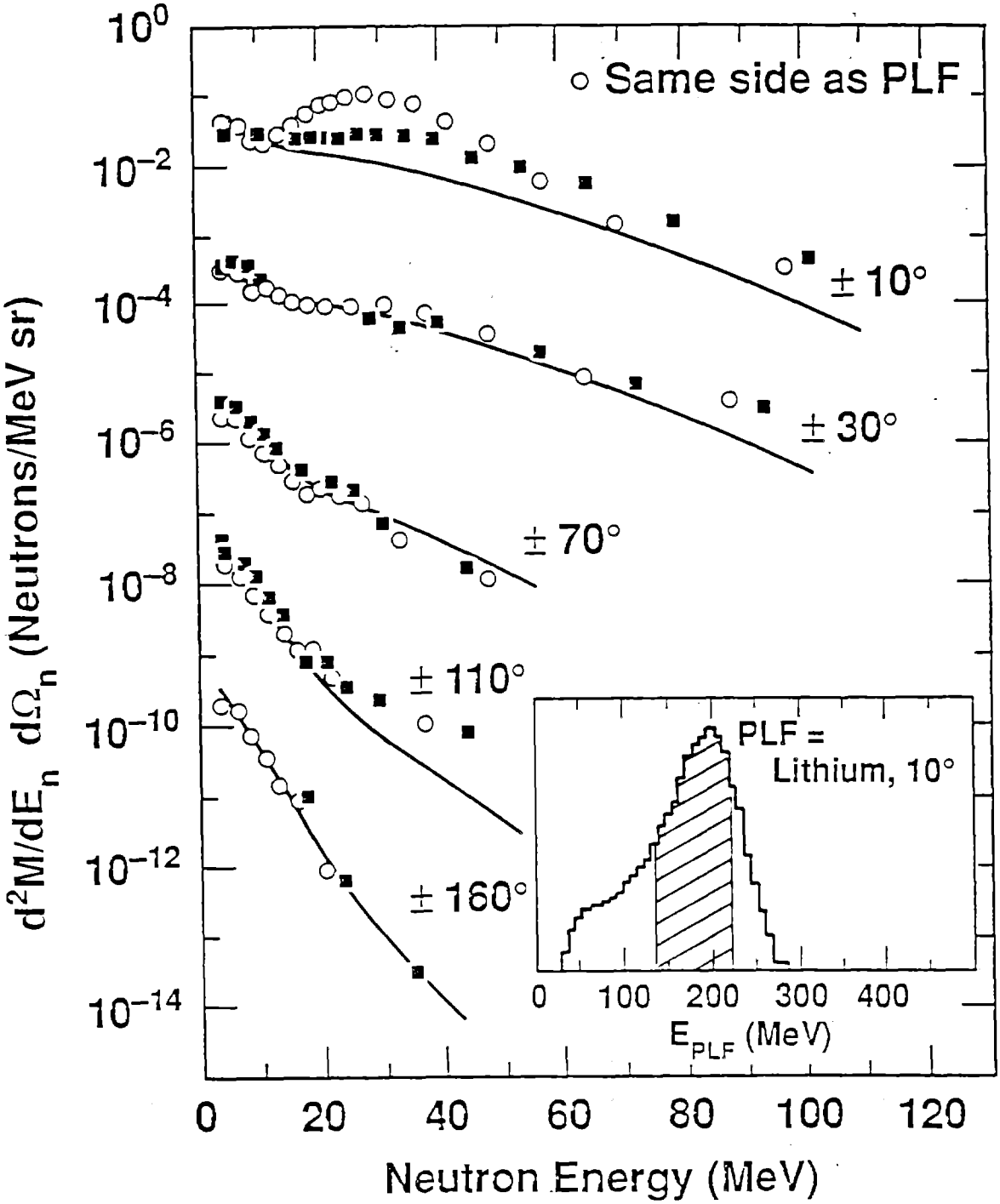

AH-115-U-4813-7

Fig. 2

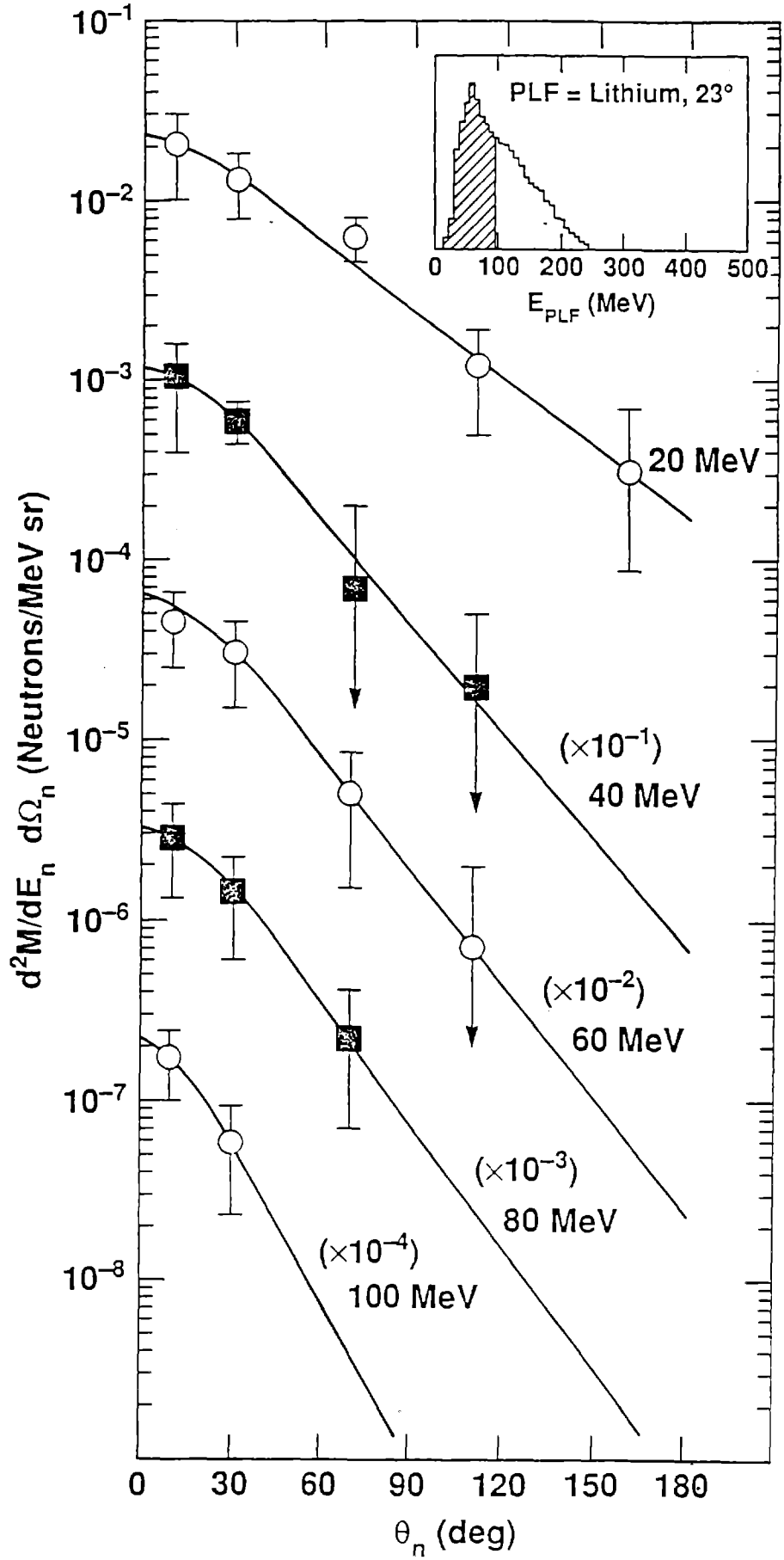
PLF = Lithium, 23°
0 100 200 300 400 500
E_{PLF} (MeV)
20 MeV
($\times 10^{-1}$)
40 MeV
($\times 10^{-2}$)
60 MeV
($\times 10^{-3}$)
80 MeV
($\times 10^{-4}$)
100 MeV
10^{-1}
10^{-2}
10^{-3}
10^{-4}
10^{-5}
10^{-6}
10^{-7}
10^{-8}
$d^2M/dE_n\ d\Omega_n$ (Neutrons/MeV sr)
0 30 60 90 120 150 180
θ_n (deg)

Fig 3

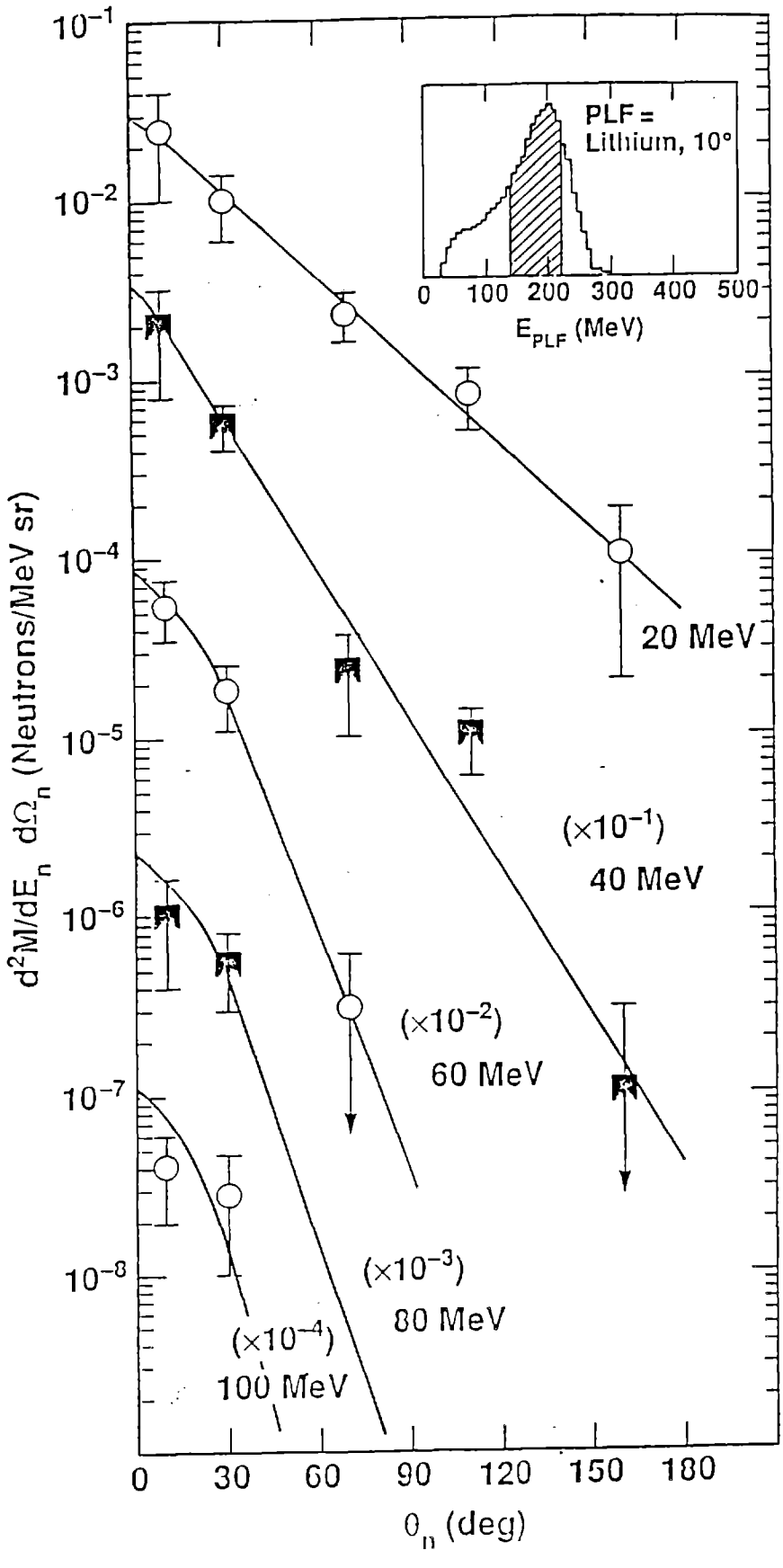
PLF = Lithium, 10°
0 100 200 300 400 500
E_{PLF} (MeV)
20 MeV
(×10⁻¹)
40 MeV
(×10⁻²)
60 MeV
(×10⁻³)
80 MeV
(×10⁻⁴)
100 MeV
$d^2M/dE_n\ d\Omega_n$ (Neutrons/MeV sr)
10^{-1}
10^{-2}
10^{-3}
10^{-4}
10^{-5}
10^{-6}
10^{-7}
10^{-8}
0 30 60 90 120 150 180
θ_n (deg)

Fig. 4

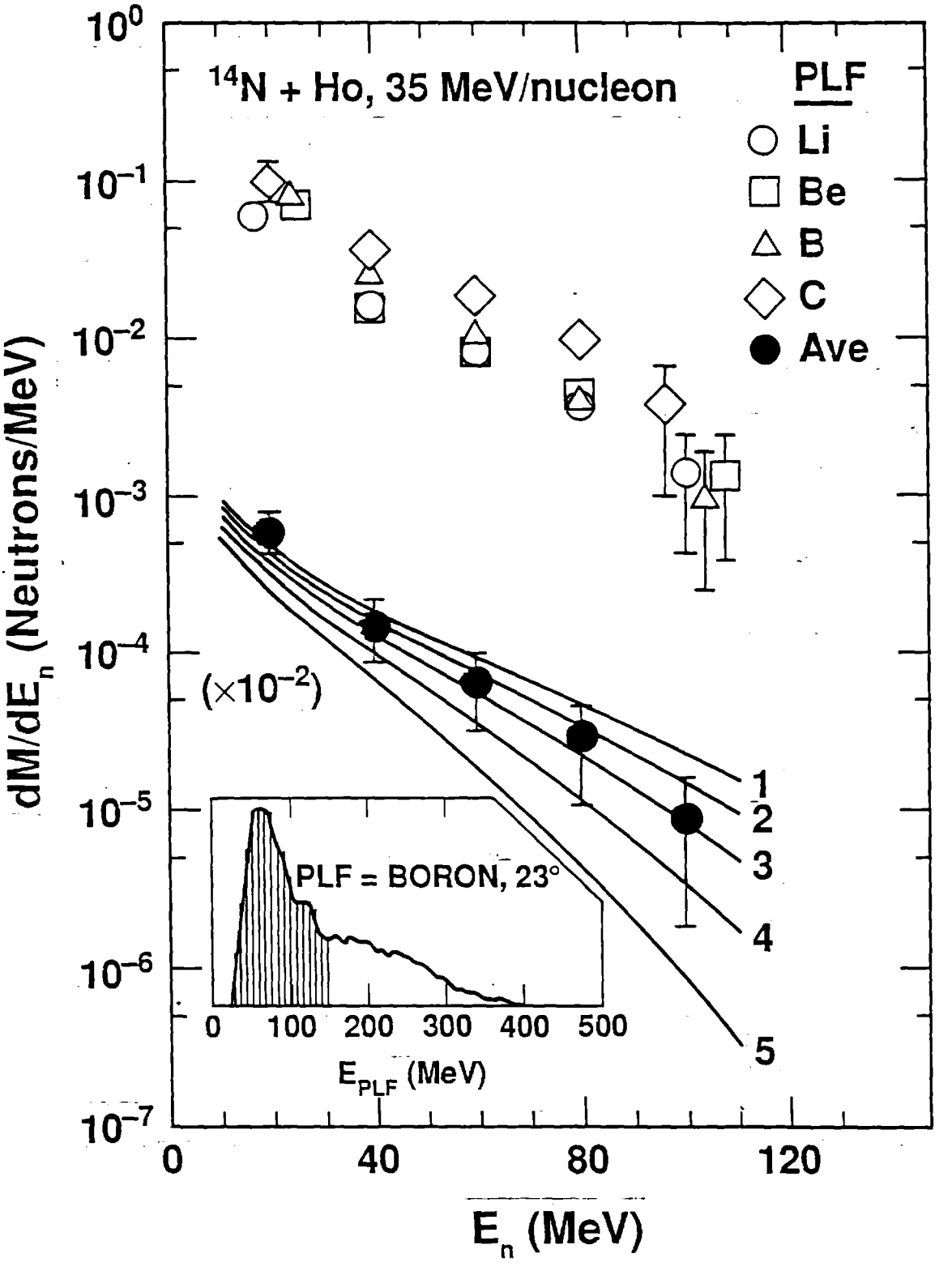
^{14}N + Ho, 35 MeV/nucleon
PLF
Li
Be
B
C
Ave
10^0
10^{-1}
10^{-2}
10^{-3}
10^{-4}
10^{-5}
10^{-6}
10^{-7}
$(\times 10^{-2})$
dM/dE$_n$ (Neutrons/MeV)
1
2
3
4
5
PLF = BORON, 23°
0
100
200
300
400
500
E$_{PLF}$ (MeV)
0
40
80
120
E$_n$ (MeV)

Fig. 5

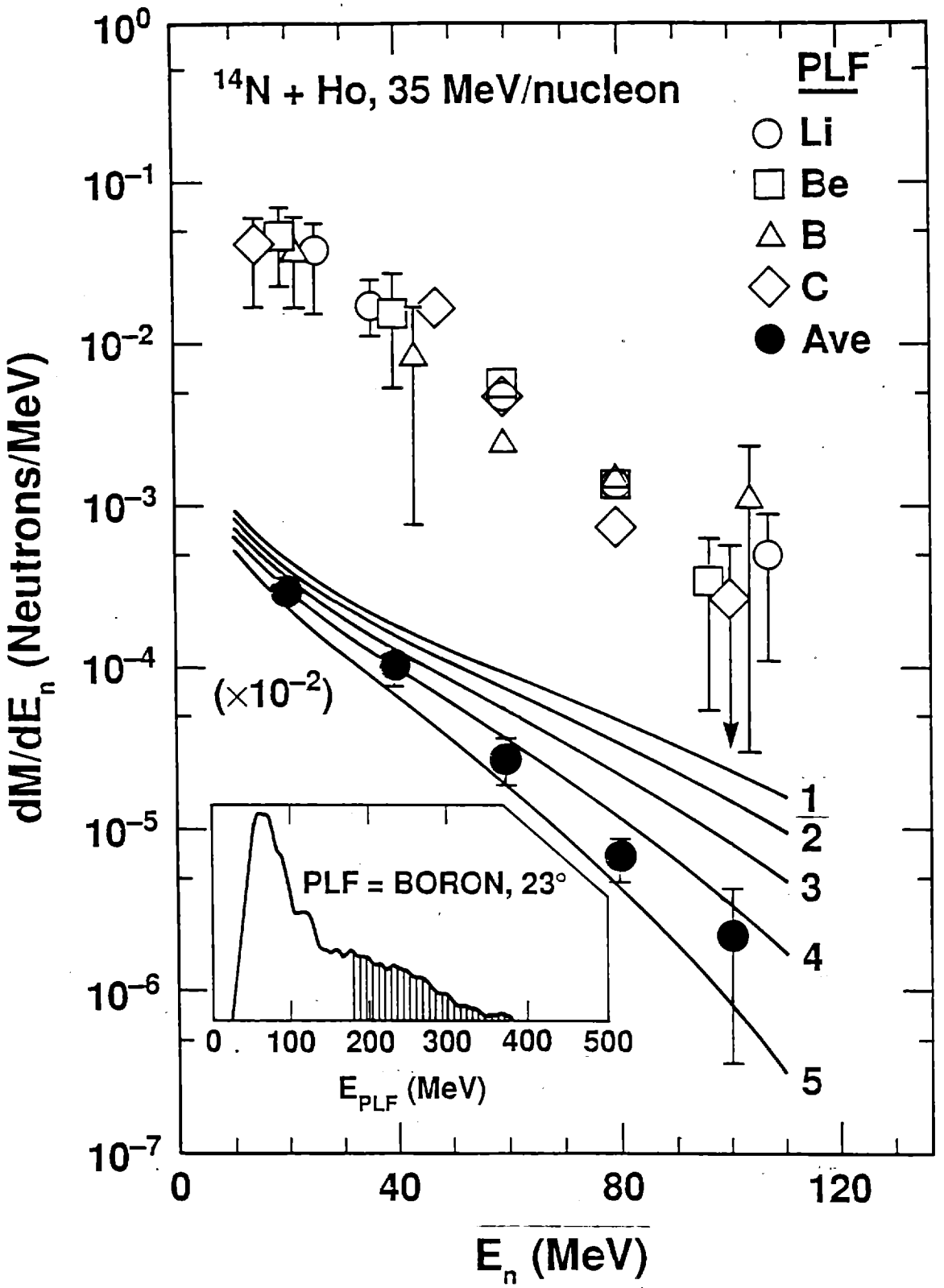
^{14}N + Ho, 35 MeV/nucleon
PLF
Li
Be
B
C
Ave
(×10^{-2})
1
2
3
4
5
PLF = BORON, 23°
0 100 200 300 400 500
E_{PLF} (MeV)
dM/dE_n (Neutrons/MeV)
E_n (MeV)
10^0
10^{-1}
10^{-2}
10^{-3}
10^{-4}
10^{-5}
10^{-6}
10^{-7}
0
40
80
120

Fig. 6

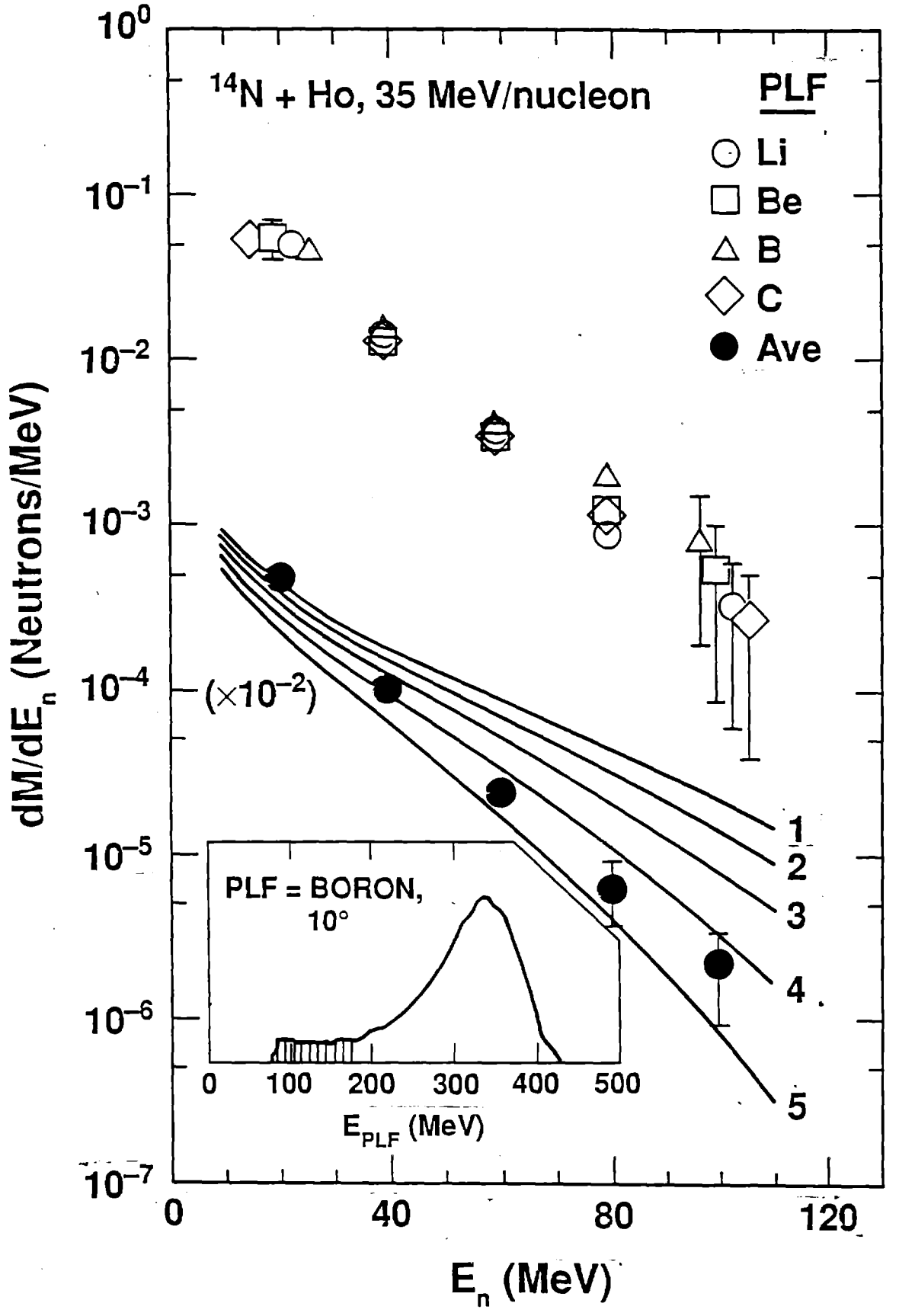
^{14}N + Ho, 35 MeV/nucleon
PLF
Li
Be
B
C
Ave
(×10^{-2})
1
2
3
4
5
PLF = BORON,
10°
0
100
200
300
400
500
E_{PLF} (MeV)
dM/dE$_n$ (Neutrons/MeV)
E_n (MeV)
10^0
10^{-1}
10^{-2}
10^{-3}
10^{-4}
10^{-5}
10^{-6}
10^{-7}
0
40
80
120

Fig. 7

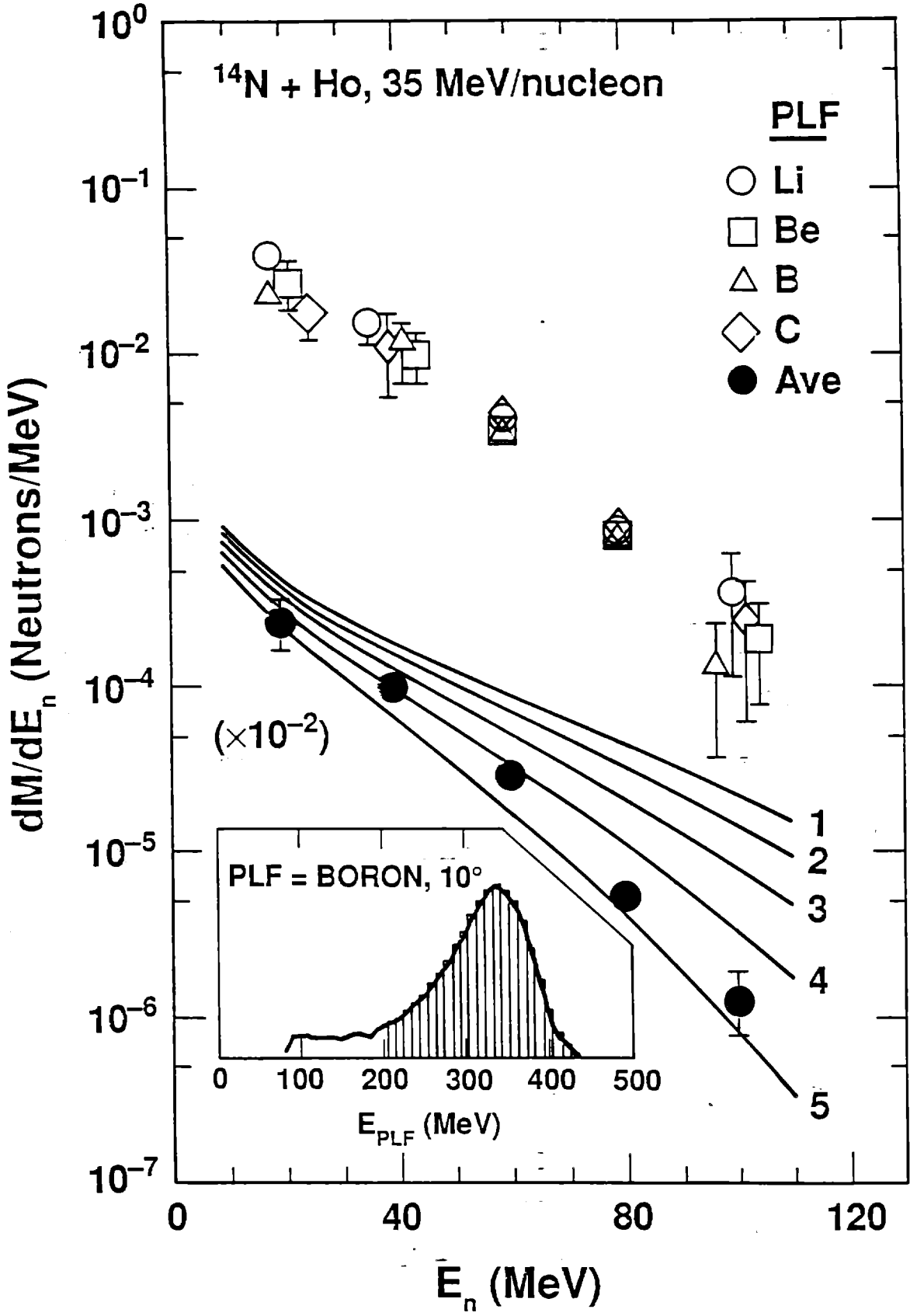
^{14}N + Ho, 35 MeV/nucleon
PLF
Li
Be
B
C
Ave
10^0
10^{-1}
10^{-2}
10^{-3}
10^{-4}
10^{-5}
10^{-6}
10^{-7}
dM/dE_n (Neutrons/MeV)
($\times 10^{-2}$)
1
2
3
4
5
PLF = BORON, 10°
0
100
200
300
400
500
E_{PLF} (MeV)
0
40
80
120
E_n (MeV)

Fig. 8

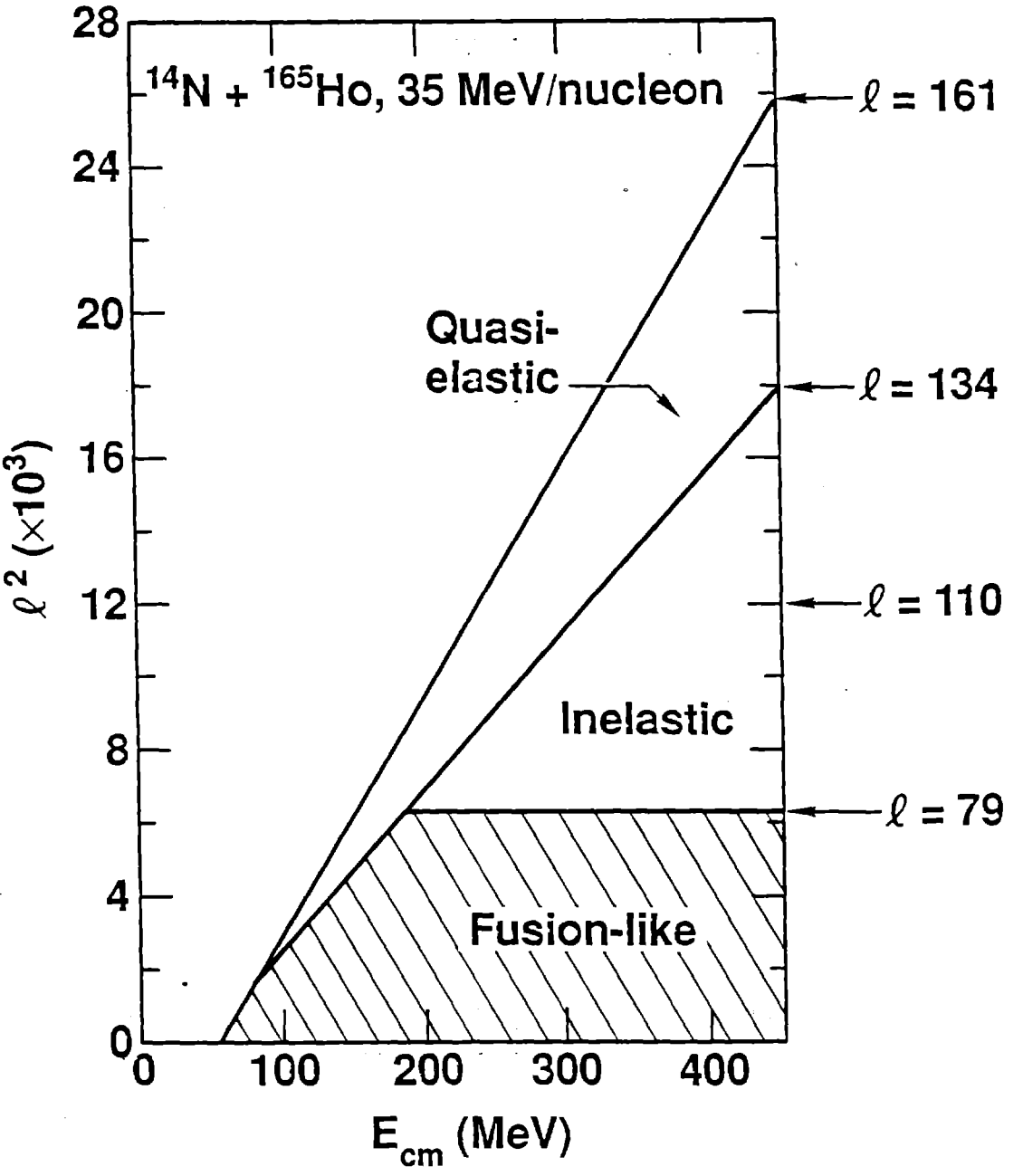
$^{14}N + ^{165}Ho$, 35 MeV/nucleon
$\ell = 161$
$\ell = 134$
$\ell = 110$
$\ell = 79$
Quasi-elastic
Inelastic
Fusion-like
ℓ^2 ($\times 10^3$)
E_{cm} (MeV)
0
4
8
12
16
20
24
28
0
100
200
300
400

Fig. 9